Available online at www.CivileJournal.org

Civil Engineering Journal

(E-ISSN: 2476-3055; ISSN: 2676-6957)

Vol. 7, No. 06, June, 2021

Performance of Ground Anchored Walls Subjected to Dynamic and Pseudo-Static Loading

Arash Saeidi Rashk Olia [1*], Mohammad Oliaei [2], Heisam Heidarzadeh [3]

[1] *Department of Civil Engineering, Kansas State University, 1701C Platt St., Manhattan, KS 66506-5000, USA.*

[2] *Department of Geotechnical Engineering, Faculty of Civil and Environmental Engineering, Tarbiat Modares University, Tehran, Iran.*

[3] *Department of Civil Engineering, Faculty of Technology and Engineering, Shahrekord University, Shahrekord, Iran.*

Received 09 February 2021; Revised 10 May 2021; Accepted 17 May 2021; Published 01 June 2021

Abstract

This study investigates the response of pre-stressed anchored excavation walls under dynamic and pseudo-static loadings. A finite difference numerical model was developed using FLAC^{2D}, and the results were successfully validated against full-scale experimental data. Analyses were performed on 10, and 20-m-height stabilized excavated slopes with 60° to 90° of inclination angle with the horizon to represent an applicable variety of wall geometries. In dynamic analysis, the statically stabilized models were subjected to 0.2 to 0.6g of the dynamic peak acceleration to evaluate the effect of ground acceleration on their performance. Furthermore, pseudo-static analyses were performed on the statically stabilized models with pseudo-static coefficients ranging from 0.06 to 0.22. The results revealed that ground anchored slopes generally showed acceptable performances under dynamic loading, while higher axial forces were induced to ground anchors in higher and steeper models. Furthermore, comparing the results of dynamic and pseudo-static analyses showed a good agreement between the two methods' predictions in the mobilized axial force along the ground anchors. Pseudo-static coefficients were then proposed to replicate dynamic results, considering the slope geometry and dynamic load peak acceleration. The results revealed that higher and steeper stabilized slopes required higher values of pseudo-static coefficients to match the dynamic predictions successfully. The results indicate that pseudo-static coefficient tend to increase with the increase in dynamic load peak acceleration in any given model.

Keywords: Geotechnical Earthquake Engineering; Slope Stability; Seismic Stability; Pre-Stressed Anchors; Pseudo-Static Coefficient.

1. Introduction

Pre-tensioned ground anchors are among the most effective technologies in stabilizing deep excavations due to their efficiency in limiting the excavation wall crown displacement more than other tieback retaining systems such as soil nailing and rock bolts. Therefore, their application has increased worldwide for both temporary and permanent excavation wall and slope stabilizations in recent decades. While this system is mostly designed for temporary stabilization of the cuts before the construction of the permanent retaining structure, it has shown some exemplary performance in earthquake-prone regions such as Athens subway stations, where the anchored wall resisted high magnitudes of ground motions, despite being designed for the minimal acceleration levels [1-3]. These incidents brought more attention to the investigation of dynamic performance pre-tensioned retaining walls.

* Corresponding author: saeidi@ksu.edu

http://dx.doi.org/10.28991/cej-2021-03091703

One of the first attempts in evaluating the dynamic behavior of pre-tensioned anchored walls was a finite element time history analyses conducted on a three-row anchored wall by Fragaszy et al. (1987) [4]. Their analyses showed that the flexibility of the pre-tensioned anchored system allows it to move in-phase with the surrounding soil, while the out-of-phase displacements of the retaining wall proved to induce high magnitudes of horizontal pressure and horizontal moments to the wall facing [4]. Further numerical parametric analyses conducted by Siller and Frawley (1992) [5] revealed that the normal stiffness of the anchor element plays an essential role in the magnitude of mobilized dynamic load, as it also decreases the dynamic displacements. Siller et al. (1991) also found that the pre-tensioning load is the most effective parameter in limiting the static displacements, while having a very insignificant impact on dynamic displacements [6]. Therefore, dynamic design instructions recommended the anchor element normal stiffness to be adopted beyond the design values resulted in the temporary static design of anchored walls.

Siller and Dolly (1992) [7] conducted a series of numerical seismic investigations on anchored wall higher number of low-capacity anchors. The result of their model revealed that pre-tensioned ground anchor stabilized walls with a higher number of low-capacity anchor elements perform more reliably under seismic loading than those with a fewer number of high-capacity anchors. Furthermore, anchored walls were also found to have more efficient seismic performance over retaining walls, especially in a higher ground acceleration up to 0.5g. Sheet piles stabilized with pre-tensioned anchors also proved to have acceptable performances under seismic loading with a peak acceleration equal up to half of the earth's gravity while experiencing high magnitudes of horizontal excess pore water pressure developed behind the wall [2].

Due to the complexity of dynamic and seismic analyses, engineers and designers have adopted the pseudo-static approach to predict the structure's response to dynamic loadings since the mid-1920s. In pseudo-static slope stability analyses, the earthquake effects are represented by constant horizontal force, which is the resultant of the active wedge mass multiplied to pseudo-static coefficient (k_h), is applied to the center of the soil active wedge mass, and the static analyses takes place considering the pseudo-static force [8]. Farhangi and Karakopuzian (2020) found that the impact of seismic hazards in natural soil slopes could be reduced by jet grouting by micropiles. They also revealed that a high correlation exists between the soil stiffness represented by $(N_1)_{60}$ in SPT test and the safety against liquefaction caused by strong dynamic loads in coarse-grained materials [9].

Oliaie and Tohodifar (2018) proposed an optimum distance of three times the pile diameter for the best seismic stabilization of slopes with sleeved and unsleeved piles [10]. More recently, Peng et al. (2020) [11] also pointed out the impact of ground motion intensity on the seismic response of rock slopes stabilized with anchors. Their findings revealed that the maximum axial force mobilized across the anchor is near the rock interface, which shows that the structural plane of the slope takes over the seismic response. The seismic performance of retaining walls with compressible inclusions was investigated by Dram et al. (2020) [12]. They applied 15 cycles of sinusoidal dynamic loads with PGA ranging from 0.1g to 0.3g. The findings from this study revealed that compressible tire shreds could decrease the permanent displacement of the retaining walls down to half. A recently-published FEM numerical study by Farrokhzad et al. (2021) on the seismic behavior of nailed excavation walls revealed the importance of nail elements' spacing and length excavation wall seismic deformation. Moreover, their analyses revealed steeper nail elements could reduce the permanent seismic wall deformation more effectively [13].

Tiwari et al. (2014) reported the outcomes of pseudo-static analyses are critically dependent on the value of k_h, which is usually recommended to be adopted roughly between 0.1 to 0.2 [14]. Komak Panah and Majidian (2013) adopted the finite difference method to predict soil nail walls' seismic behavior. The result of their study showed that by adopting the proper k_h, a good agreement could be observed between numerical seismic and numerical pseudo-static analysis results [15].

Previous studies revealed the flexible performance of anchored walls under seismic loads and the pseudo-static approach's effectiveness in dynamic slope stability analyses [1-3, 15]. While numerical analyses are powerful tools in computational modeling of geo-mechanical problems, they require considerable computational power and are time-consuming procedures. In the case of dynamic analyses performed in this study depending on the model's dimensions, it took 8 to 32 hours for each analysis. On the other hand, numerical pseudo-static analyses can be performed in several minutes. If an accurate pseudo-static coefficient is implemented is capable of replicating dynamic analysis results. Also, previous studies on pseudo-static analyses suggested using the value 0.1 to 0.2, which is a wide range and can lead to a big difference in the mobilized internal and external forces and dynamic displacements. Additionally, this wide range of pseudo-static coefficients (k_h) neither considers the type of the slope and the supporting retaining structure nor the height and the inclination of the slopes and the seismic load intensity. To this end, this study aims to suggest k_h values for the pre-stressed-ground-anchored retaining structures to enable more accurate prediction of dynamic mobilized anchor forces considering model geometry, including height and slope inclination, as well as ground motion intensity. In order to accomplish this, six numerical anchored excavation models with 10m and 20m height and slope inclinations of 60°, 75°, and 90° are developed and statically stabilized. Then all of these models are subjected to two dynamic loads, each of which having Peak Ground Acceleration (PGA) ranging from 0.2g to 0.6g. Pseudo-static analyses are conducted

by applying k_h ranging from 0.06 to 0.22. At the end, the results of dynamic mobilized forces along the anchors are bracketed by outcomes numerical pseudo-static analyses to propose the most valid k_h for that specific geometry and PGA. Furthermore, the numerical model is validated against full-scale experimental data in predicting the response of pre-tensioned anchored wall excavation with good agreements. Figure 1 shows a flowchart of the research methodology employed in this study.

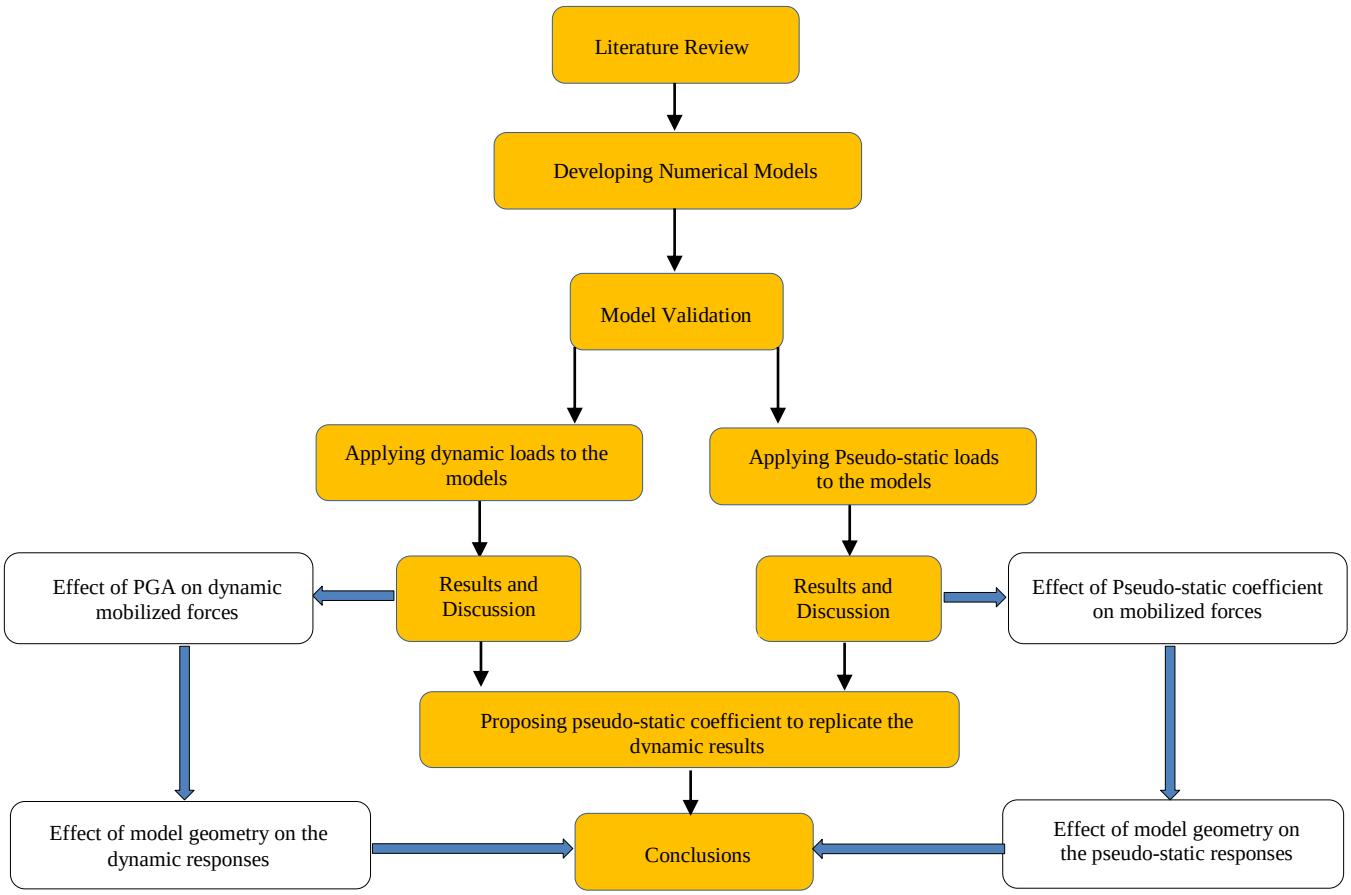

Figure 1. Research methodology flowchart

2. Model Description

All numerical models were developed with the Finite Difference Method (FDM) using FLAC^{2D}. An overall of six excavations representing 10m and 20m height excavations with different face angles of 60°, 75°, and 90° with the horizon was developed representing a wide range of excavation geometry with mild to steep face inclinations. Models will be denoted with two-part names as H10-i75 representing the model with 10m height and 75° herein.

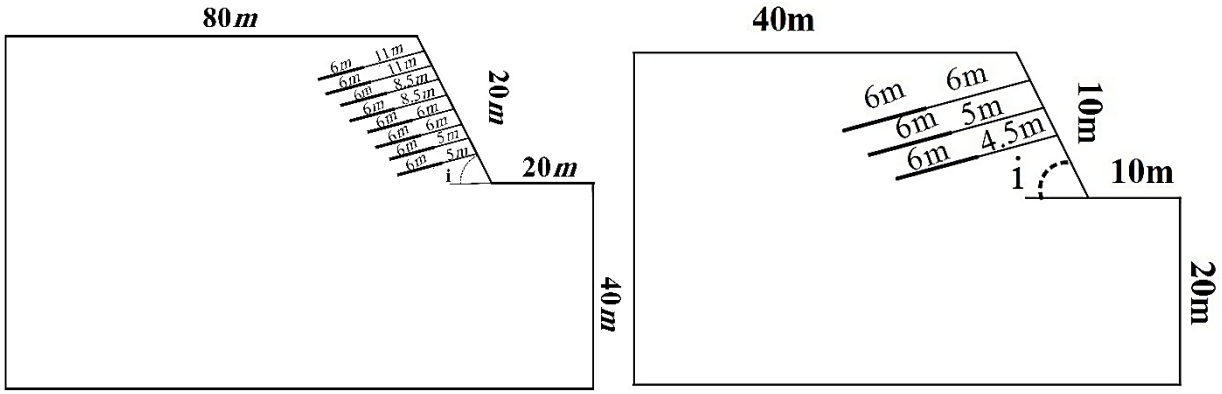

(a) 20 meter-height model **(b) 10 meter-height model**

Figure 2. Schematic models' geometry and anchors arrangements (not scaled)

After a series of trial and error in developing models with different anchor lengths, horizontal and vertical distances and lock of loads the final arrangements shown in Figure 2 were found to best satisfy the minimum static factor of safety equal to 1.5 recommended by Federal Highway Administration Ground Anchors and Anchored System for permanent application of ground anchors [16]. To simulate a three-Dimensional problem in two dimensions, Donovan et al. (1984) [17] suggested linear scaling of material properties. This simple and convenient approach of distributing elements' discrete effect over the distance between elements in a regularly spaced pattern. This is accomplished by dividing the element properties by the distance between elements. Therefore, the anchors' pre-tensioning load was set to 450 kN for all anchors in the design was scaled to 150 kN for 10 meter-height excavations due to 3 meters horizontal spacing of anchors and 180 kN for 20 m excavations due to 2.5 m meters horizontal spacing.

Kulhemeyer and Lysmer (1973) [18] suggested that zone dimensions in a finite difference analysis be one-tenth to one-eighth of the input wavelength's highest frequency component for proper wave propagation in dynamic analyses. In the present study, the wavelength for H-1 and H-2 harmonic loads were 55 and 46.87 meters, respectively; hence the dimensions of the zones are 25 cm, and 50 cm in the models of 10m and 20m are qualified for the proper wave propagation condition for both models.

2.1. Soil

Tehran alluvium, classified as SM according to the Unified Classification System, was chosen for the analyses. The hyperbolic Duncan-Chang model was chosen to simulate the soil behavior. This nonlinear model considers the stress level effects on the stiffness and strength of the soil [19]. In addition, it provides the possibility of modeling unloading and reloading of the along a different path from the loading path. The tangent Young's modulus E_t, the initial slope of the stress-strain curve in the hyperbolic model, is defined as

$$E_t = \left[1 - \frac{R_{f(1-sin\varphi)(\sigma_1-\sigma_3)}}{2(c\ cos\varphi + \sigma_3\ sin\varphi)}\right]^2 K * P_a \left(\frac{\sigma_3}{P_a}\right)^n \quad (1)$$

Where R_f is the failure ratio, K is the initial tangent Young's modulus factor; P_a is the atmospheric pressure, φ is the friction angle of the soil, c indicates the cohesion of the soil, σ_1, and σ_3 are major and minor main stresses, and n is the stress influence component [19-20]. Accordingly, the tangent Bulk modulus and Young's modulus for Unloading-Reloading (ur) are expressed as

$$B_t = K_b * P_a \left(\frac{\sigma_3}{P_a}\right)^n \quad (2)$$

$$E_{ur} = K_{ur} * P_a \left(\frac{\sigma_3}{P_a}\right)^n \quad (3)$$

Where K_b is the bulk modulus factor, and K_{ur} is unloading-reloading modulus factor. The soil model parameters for Duncan and Chang constitutive model were calibrated and represented [21, 22]. In Table 1 the parameters were derived based on calibration of the model prediction against triaxial and direct shear test results.

Table 1. Soil parameters for sand [21, 22]

Parameter	*K*	*n*	R_f	φ	*C (kPa)*	K_{ur}	K_b	γ (kN/m^3)
value	285	1	0.9	38°	10	600	474	19.7

2.2. Structural Elements

Beam elements, which are capable of resisting axial forces and bending moments, were implemented in order to model reinforced concrete for the excavation facing flexural strength for a 30 cm reinforced concrete wall facing (EI) was suggested to be 29.9 MPa [13,15, 23]. Cable elements were used to simulate high resistance steel strands with ultimate tensile strength (f_u) of 1860 MPa used by Gazetas et al. 2016 [2].

2.3. Boundary Conditions

Boundary conditions play essential roles in both static and dynamic analyses. Their role is considerably more critical in dynamic studies as the reflection of dynamic waves from boundaries could result in numerical errors in model response. The boundary conditions of the model were taken as full-fixities at the base of the model with vertical rollers on the lateral sides of the model except for models for static and pseudo-static analyses. Free-field boundary conditions in finite difference numerical modeling using FLAC are a practical approach to prevent wave reflection and eliminate the boundary effects in dynamic analyses, which were specified along the model's lateral edges [24].

2.4. Damping

Using elasto-plastic soil models provides sufficient hysteretic damping when dynamic shear stress exceeds soil plastic yield resistance, and plastic deformations take place. However, further damping is required in an elastic state. Rayleigh damping with a 3% ratio was implemented to the soil profile with the central frequency of damping set to the fundamental frequency of the structure suggested by FLAC manual [24].

3. Loading Description

3.1. Construction Stage (Static) Analyses

Since plastic deformations and stress redistribution affects the total excavation results, the actual excavation sequences should be simulated prior to dynamic and pseudo-static analyses. To this end, after the mesh generation, excavation to the first anchor level is modeled as shown in Figure 3b. It should be noted that the mesh dimensions are finer at regions where the anchors are meant to be installed to provide more accurate calculations. The anchor element installation is shown in Figure 3c, and after that, the pre-tensioning load is applied to the anchor element. As illustrated in Figure 3d, the pre-tensioning load decreases gradually in the bonded portion of the anchor and does to zero at the end of this area while stays constant in the un-bonded area where the soil and anchor element are arranged to have zero interaction. These steps are repeated to the point the desired excavation depth is reached.

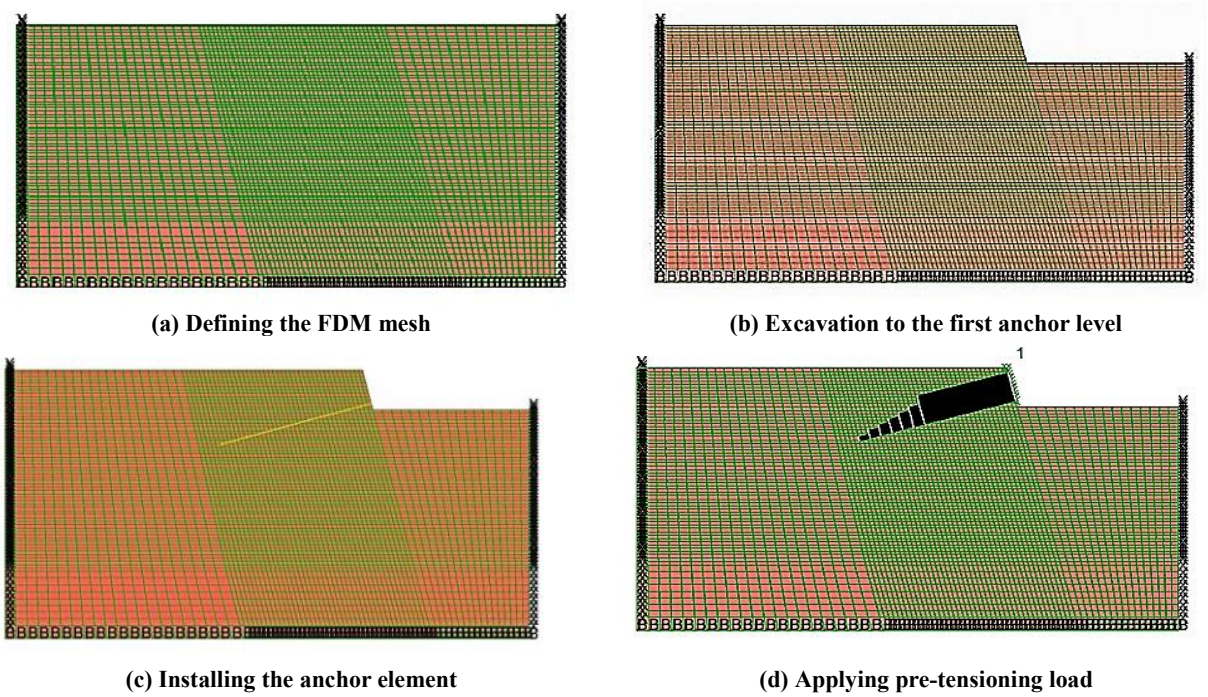

(a) Defining the FDM mesh **(b) Excavation to the first anchor level**

(c) Installing the anchor element **(d) Applying pre-tensioning load**

Figure 3. stages of numerical modelling of the anchored excavation in FLAC

3.2. Dynamic Loading

Dynamic loads were chosen in a way that represent the main characteristics of real earthquakes in which the acceleration increases gradually and then decreases towards the end of the earthquake. Horizontal acceleration time histories as presented in Equation 5 were applied to the model's base boundaries.

$$a = \sqrt{\beta e^{-\alpha t} t^{\xi}} sin\ 2\pi ft \quad (5)$$

Where f is the dynamic load frequency, and α, β, and ζ are the coefficients determining the shape and number of cycles in dynamic loading. Based on the parameter values presented in Table 2, harmonic acceleration time histories H-1 and H-2 representing moderate and severe earthquakes, respectively scaled to 1 m/s^2 acceleration are shown in Figures 4-a and b. In this study, models are subjected to H-1, and H-2 scaled to 0.1g to 0.6g, where g is the acceleration of the gravity (9.81 m/s^2).

Table 2 Specifications of selected harmonic loads

Harmonic load type	f	α	B	ζ
H-1	5	5	5.75	11.8
H-2	6	3.1	0.2	11.8

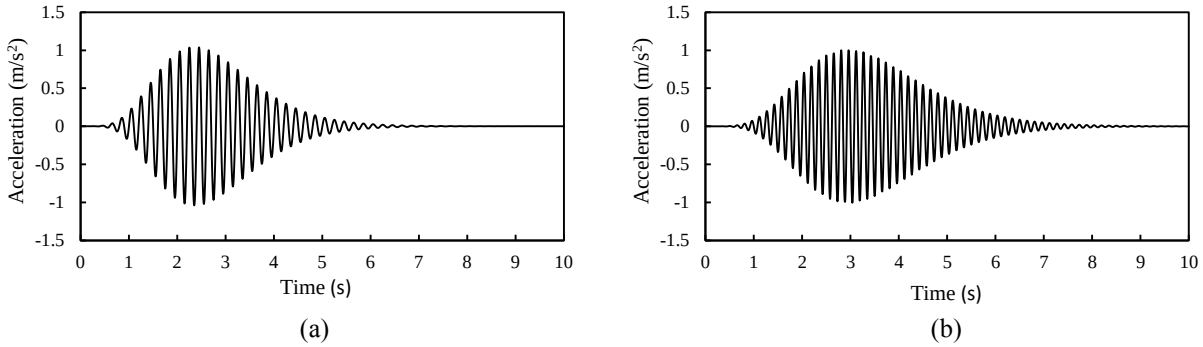

Figure 4. Harmonic load a) H-1 b) H-2 (scaled to 1 m/s²)

3.3. Pseudo-static Analyses

The pseudo-static approach is a conventional method to simulate the seismic effects of earthquakes on excavations. In the limit equilibrium method, the seismic effects are simulated by a horizontal force (F_h) equal to the product of the active soil weight W and the earthquake horizontal coefficient k_h as the following:

$$F_h = k_h.W \tag{6}$$

If W is broken into its constituents, mass (m) and g, then Eq. 6 could be rewritten as

$$F_h = (k_h.g).m \tag{7}$$

The pseudo-static analyses were conducted by implementing this concept by changing the magnitude and angle of the applied gravity acceleration (g) in FLAC and converting it to virtual gravity acceleration (g'). Figure 5 further illustrates how g' results from based on g and k_h [15].

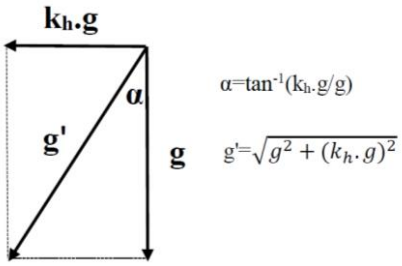

Figure 5. Acceleration resultants of the virtual gravity

3.4. Model Validation

The anchored excavation numerical model developed with FLAC^{2D} was validated against the full-scale instrumented anchored wall constructed and tested at the National Geotechnical Experimentation Site on the riverside campus of Texas A&M University. This wall was 60 m in length and 7.5 m in height. It was built by driving H piles in a line on 2.44-m center for one part of the wall and by drilling and grouting, H piles in a line on 2.44-m center for the other part of the wall. As it is shown in Figure 6a, half of the anchored wall was stabilized with only one row of anchors, while the other half had two rows of anchor reinforcement. The steel H piles were HP 6 * 24 section, 9.15 m in length, embedded 1.65 m below the bottom of the excavation. The wall facing between the H-piles was stabilized by installing wood lagging boards.

The soil profile in the site was a 13-m-thick layer of medium dense, fine silty sand deposited in a river environment; 50,000 years ago, and underlain by a 40-million-years-old hard shale. The engineering properties and the geology of this sand deposit have been determined in detail as part of the National Geotechnical Experimentation Site program [25, 26]. The following average properties of the sand are a total unit weight of 18.5 kN/m^3, standard penetration test blow count increasing from 10 blows per 0.3 m at the surface to 27 blows per 0.3 m at the bottom of the piles, borehole shear friction angle of 32° with no cohesion, cone penetration test point resistance of 7 MPa, PMT modulus of 8 MPa, and PMT limit pressure of 0.5 MPa. The water level is 9.5 m below the top of the wall.

The two-row anchor wall was used to calibrate the numerical model. The same numerical values and parameters used by Briaud and Lim (1999) in FEM modeling of the wall was implemented in the FDM model as shown in Table. 3.

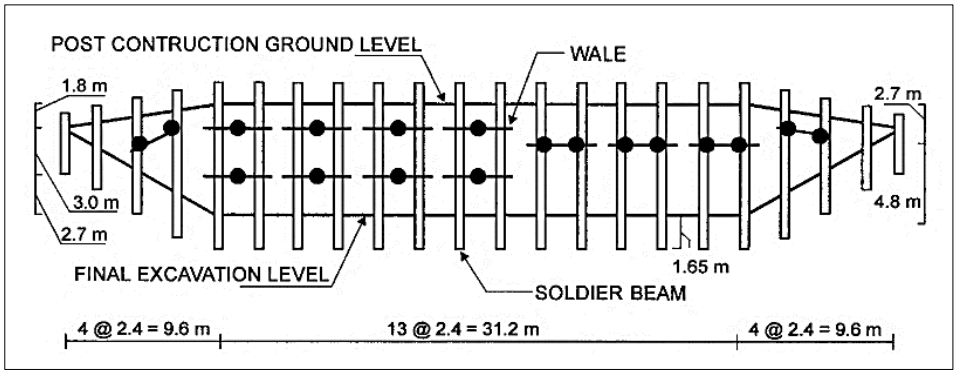

(a) Elevation View

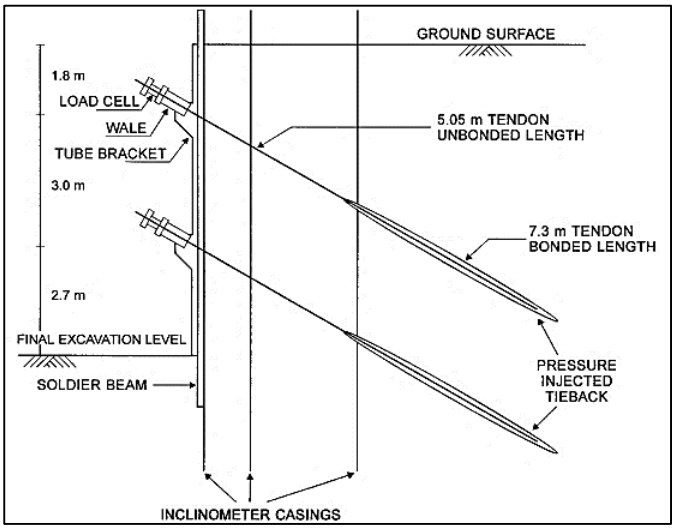

(b) Two-row anchored wall, section view

Figure 6. Texas A&M University anchored wall [25]

Table 3. Parameters used in numerical model of Texas A&M University anchored wall [25]

Data	Parameters	Values
Soil	K	300
	n	0.85
	R_f	0.93
	φ	32°
	$C(kPa)$	0
	K_{ur}	1200
	K_b	272
	$\gamma\ (kN/m^3)$	18.5
	K_0	0.65
Anchors	Unbonded length (m)	5.05
	Bonded length (m)	7.3
	Lock-off load row 1 (kN)	183.2
	Lock-off load row 1 (kN)	160
	Stiffness (kN.m)	19,846
	Angle of Inclination (β)	30°
Wall	Wall height (m)	7.5
	Length of soldier-pile(m)	9.15
	Pile Embedment length (m)	1.65
	Flexural stiffness, EI (kN.m^2)	11,620
	Axial stiffness EA (kN)	1.47 * 106
	Elasticity modulus (GPa)	210

The wall displacement, moment, and axial force resulted from the numerical model, and the field test is depicted in Figure 7. As Figure 7a demonstrates, both numerical and experimental approaches show the maximum displacement at the wall crown and the minimum at the wall base with an acceptable agreement. The numerical model also shows good

agreement in predicting the axial force and moment along the wall. Both models confirm that the maximum moment is developed at the anchor level, while the maximum axial force is generated at the lower anchor level.

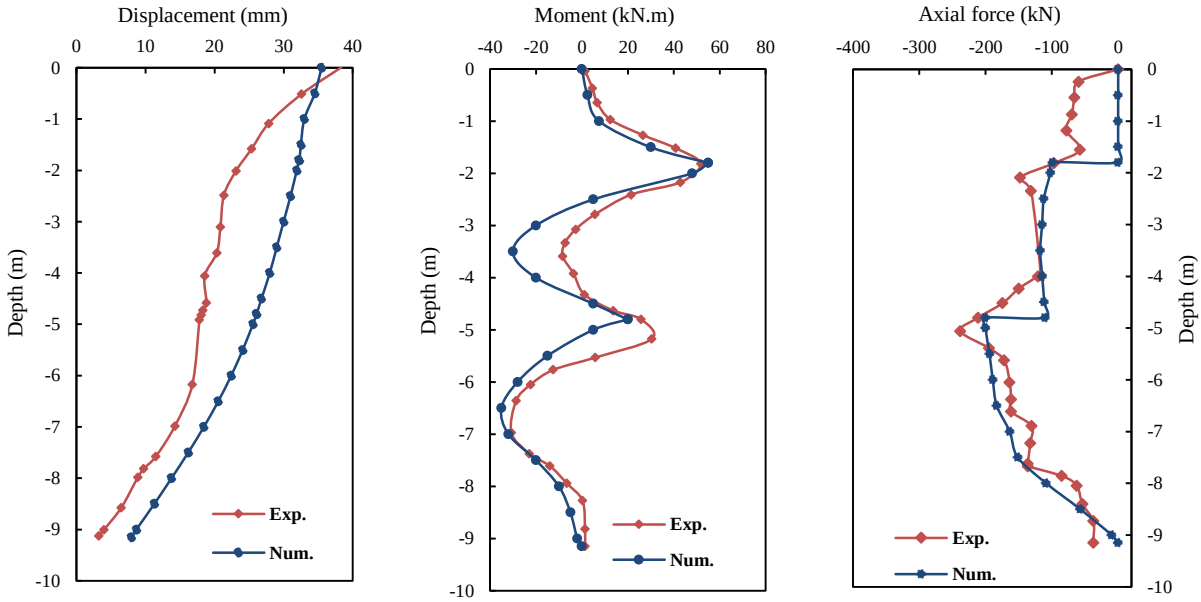

(a) wall deflection **(b) wall moment** **(c) wall axial force**

Figure. 7 Comparison of numerical results and field data

4. Results

4.1. Dynamic Analyses Results

The axial forces mobilized in anchors at the end of dynamic analyses, and pseudo-static analysis served as the basis for comparing the dynamic and pseudo-static analyses. As shown in the Figure 8 the axial load in the anchors also demonstrates the harmonic behavior of the dynamic load applied to the model during the excitation time. The stable mobilized load at the end of the dynamic excitation remains in the anchor element as the dynamic load. The axial load time history of the anchor element demonstrated the same frequency as the dynamic load applied to the model.

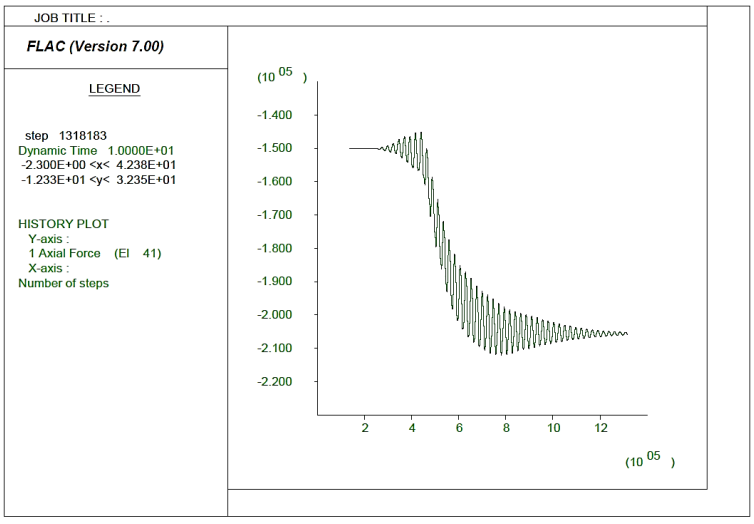

Figure 8. Anchor element axial force time history under load H-2

Figures. 9 through 11 represent the anchors' dynamic forces for 10m models subjected to H-1 and H-2 dynamic load with increasing PGA from 0.2g to 0.6g. As expected, the dynamic loading resulted in an increase in mobilized force in ground anchors. The increase of the PGA results in a higher magnitude of mobilized dynamic forces in ground anchors. The slopes' angle also proved to play an important role in the value of mobilized force, and the anchors in vertical models (i-90) experienced the highest dynamic force increase, while lower magnitudes of dynamic force were generated in i-75s and i-60s, respectively. Dram et al. (2020) [12] observed the spike pattern in the horizontal earth pressure at the one-sixth of the bottom of wall height in their FEM model which also emerges here as the dynamically mobilized anchor

force. This pattern is more noticeable in the results of 20m models in Figures 12 through 14. The lowest anchor, located at the one-sixth of the bottom of wall height, undergoes a much higher dynamic load than the anchor elements above that. Farrokhzad et al. (2021) [13] also reported the same pattern in soil nails, but the percentage of the mobilized dynamic force at the lowest soil nail is considerably less than what was observed in this study. The reason for that could be the higher capacity of ground anchors compared to soil nail elements as well as higher PGAs implemented in this study compared to Tabas earthquake time history applied to the FEM soil nail model.

In terms of the impact of the PGA on the horizontal earth pressure and mobilized anchor force, it is observed that the axial troops in anchors in this study are more impacted by the increase in the PGA comparing to the horizontal earth pressure reported by Dram et al. (2020) [12]. It can be concluded that the flexural stiffness of the retaining structure impacts the dynamic horizontal pressure and forces developed at the retaining wall. However, it should be mentioned that the retaining structure height may also be an important factor in this regard since it is noticed that in the 20m models, the impact of PGA increases and the anchors tend to undergo higher tension with ground motion intensity increased compared to what observed in 10m models in Figures 9 through 11.

Also, it was observed that with the suggested minimum factor of safety of 1.5 no failure took place in any of the models which validates the recommended Factor of safety by FHWA. However, should any failure or rupture have happed in the dynamic or pseudo-static analyses suggesting any valid coefficient became impossible. It also validates authors choice for material strength and parameters to develop dynamically-resistant enough models to resist dynamic loads to this intensity.

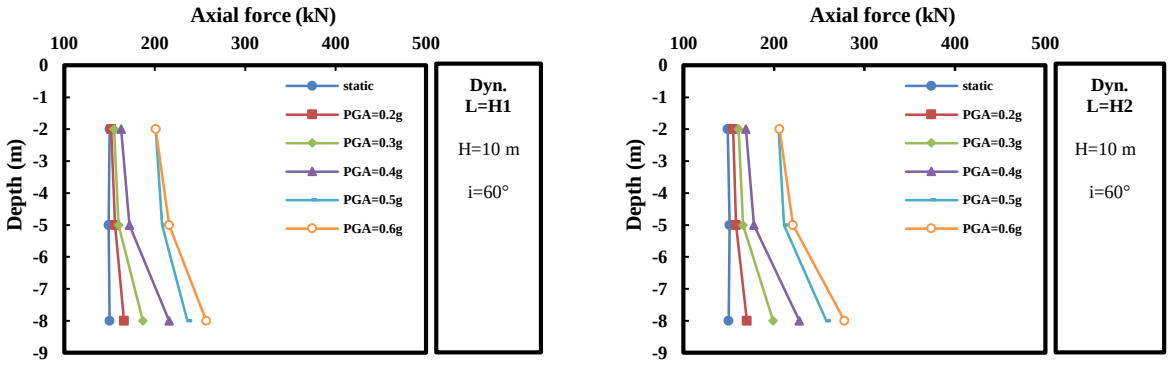

Figure 9. Dynamic axial forces of the anchors along the height of the model H10-i60

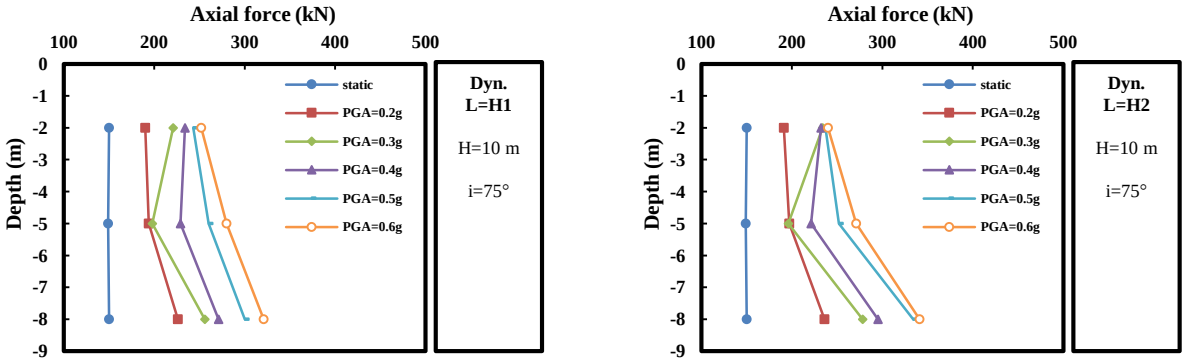

Figure 10. Dynamic axial forces of the anchors along the height of the model H10-i75

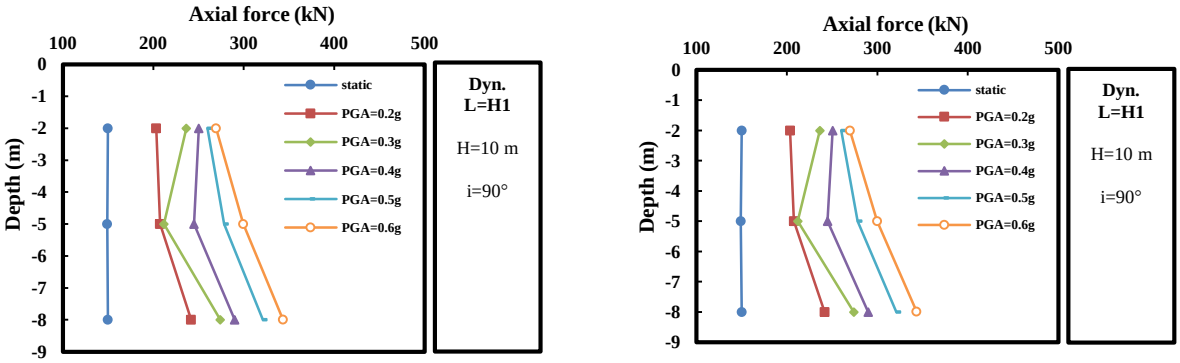

Figure 11. Dynamic axial forces of the anchors along the height of the model H10-i90

Similar to 10 models, dynamic forces along the anchors increase with PGA and have higher values for more steep excavations. The anchors' dynamic loads in each model increase from the top to the bottom of the excavation, with more intensity the lower 3 anchors with the maximum mobilized dynamic force in the lowest anchor for all models. The highest difference of dynamic forces generated with different Ground acceleration was generated from PGA=0.4g to PGA= 0.5g in both 10 and 20 m models.

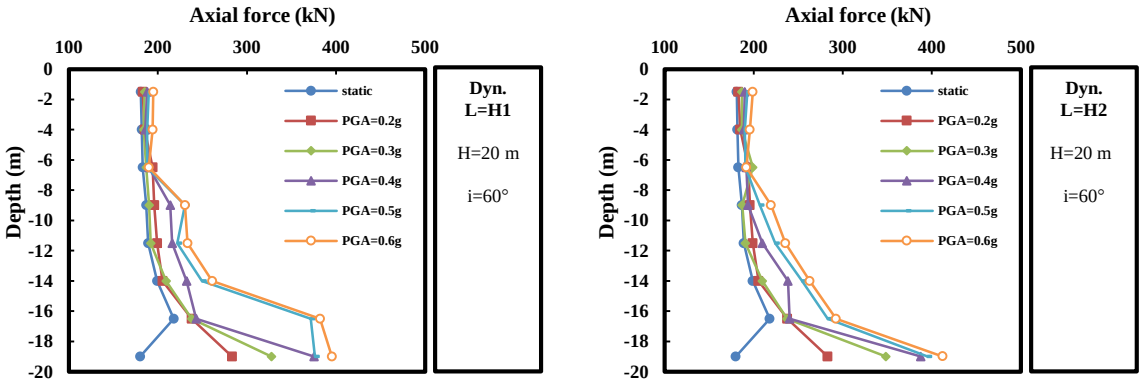

Figure 12. Dynamic axial forces of the anchors along the height of the model H20-i60

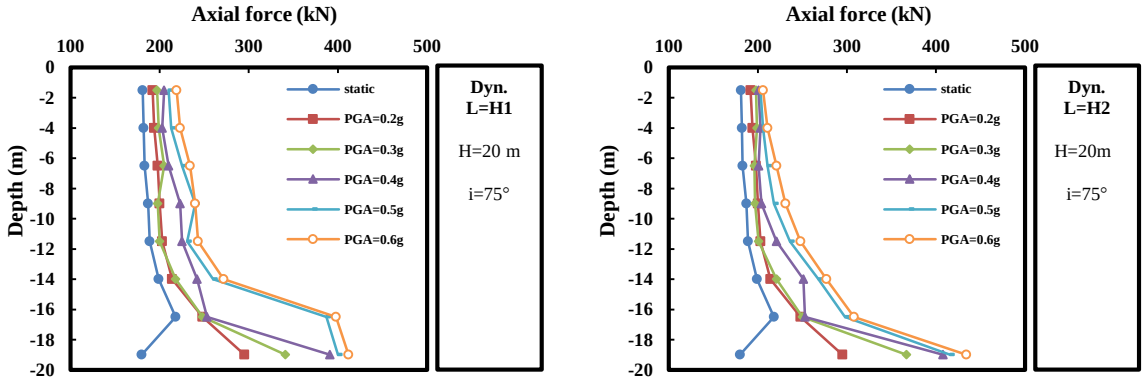

Figure 13. Dynamic axial forces of the anchors along the height of the model H20-i75

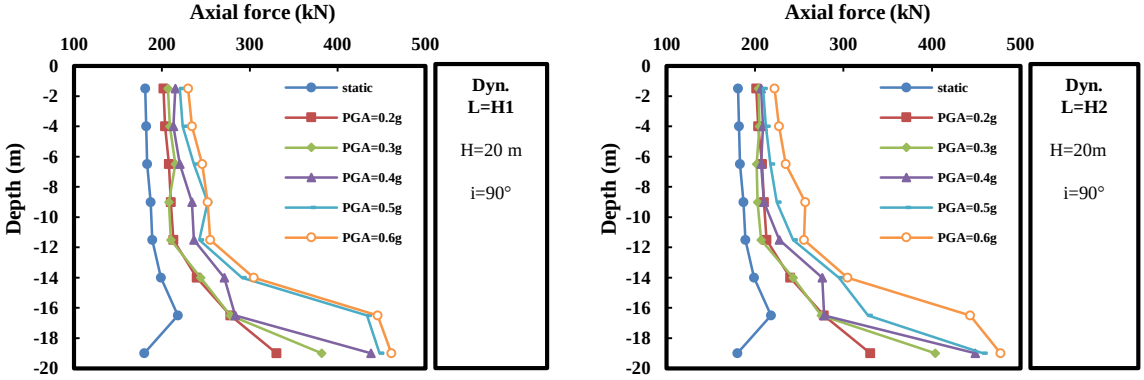

Figure 14. Dynamic axial forces of the anchors along the height of the model H20-i90

In this study, anchors were designed and modeled to resist the highest mobilized dynamic load. Therefore, the cross-section of all the ground anchors set to withstand 482 kN mobilized in the bottom anchor of model H20-i90, under dynamic load H-2 with 0.6g PGA.

4.2. Pseudo-static Analyses Results

Pseudo-static analyses were conducted to replicate the dynamic force mobilization in anchors. The dynamic forces were the criterion for selecting the values of k_h for models so that the axial forces induced in pseudo-static analyses would totally encompass the axial forces induced under all dynamic loading scenarios. Therefore, 10m models were subjected to pseudo-static coefficients k_h =0.06 to k_h =0.2, and 20-m-models were subjected to k_h =0.12 to k_h = 0.22 under pseudo-static analyses.

Axial forces induced in pseudo-static analyses showed a similar pattern to dynamic axial forces along the models' depth, as shown in Figures 15 through 20. Similar to dynamic analyses, pseudo-static induced forces in anchors increase

with depth, with the maximum values in the lowest anchors in all models. Three anchors at the bottom in 20m models witnessed drastic changes compared to anchors above them in each model, and an increase in pseudo-static coefficient (k_h) led to raising in induced pseudo-static axial force in anchors in models. The same behavior in the mobilization of noticeably higher axial force in lower anchors is also seen in pseudo-static analysis results. The top four anchors in 20-m-height slopes in both dynamic and pseudo-static analyses revealed the least dependency on either PGA or pseudo-static coefficient and PGA, while in 10-m-height models, the anchor forces increase more noticeably top and middle anchors, which is due to the higher horizontal displacement of the anchors in 10-m-model comparing to the 20-m- model and highlights the role of horizontal spacing in the dynamic and pseudo-static response of anchored walls since the vertical spacing were chosen the same for both models in the design and modeling. k_h =0.22 causes the highest deviation from the lower pseudo-static coefficients in 20m models. These same patter behaviors are observed in dynamic analyses under PGA higher than 0.4g. This implies that since earthquakes with PGA higher than 0.4g are not considered probable scenarios for earthquakes k_h higher than 0.2 is far from recommended values for retaining structures pseudo-static analyses.

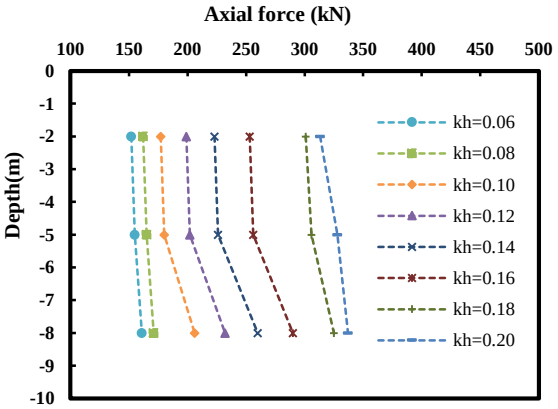

gure 15. Pseudo-static axial forces of the anchors along the height of the model H10-i60

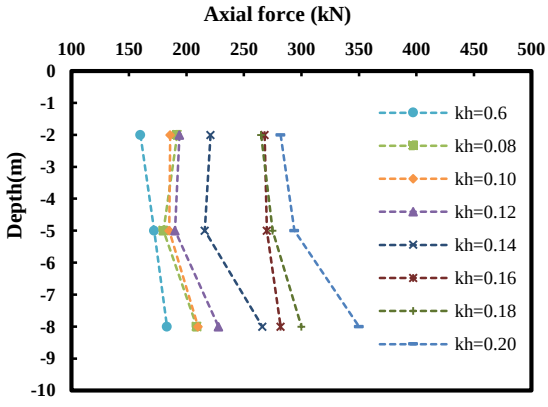

gure 16. Pseudo-static axial forces of the anchors along the height of the model H10-i75

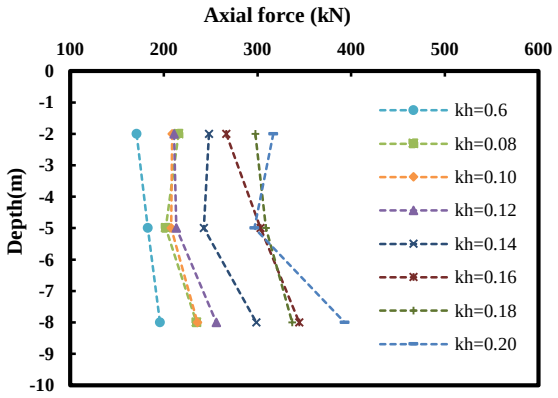

Figure 17. Pseudo-static axial forces of the anchors along the height of the model H10-i90

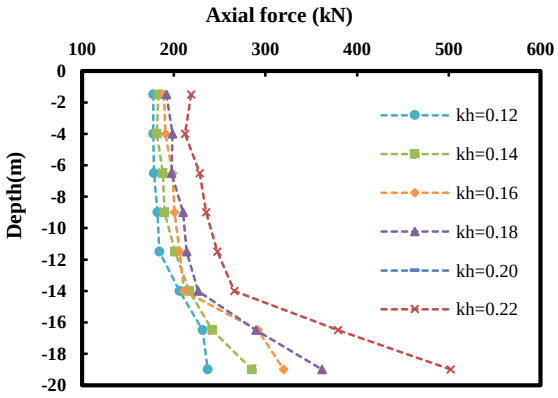

Figure 18. Pseudo-static axial forces of the anchors along the height of the model H20-i60

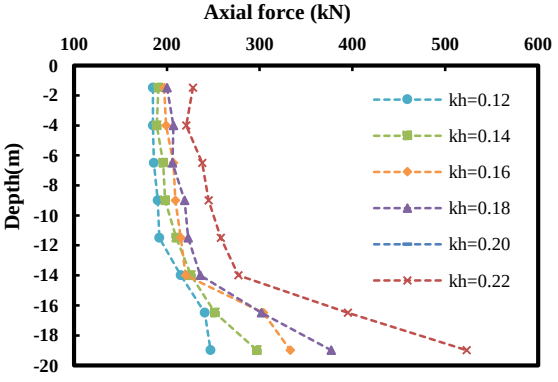

Figure 19. Pseudo-static axial forces of the anchors along the height of the model H20-i75

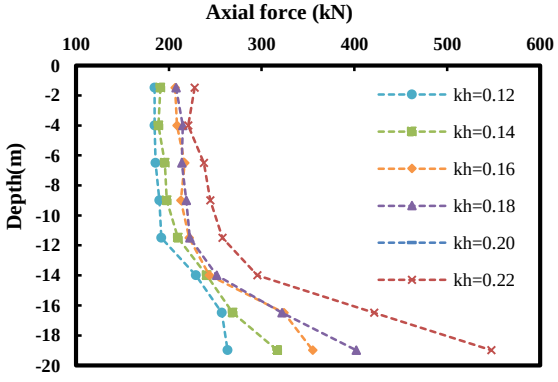

Figure 20. Pseudo-static axial forces of the anchors along the height of the model H20-i90

4.3. Pseudo-static Coefficient

Based on the induced axial forces in pseudo-static and dynamic analyses, k_h values to replicate the dynamic induced axial force with pseudo-static axial forces along the depth of each model are presented in Table 4. Minimum and maximum values of k_h that reproduced the dynamic response of the model were then averaged to have the unique pseudo-static coefficient in each case.

β value as defined in Equation 8 represents the relationship between the maximum acceleration of the dynamic load and the pseudo-static coefficient, where a_{max} is the maximum acceleration in the dynamic load and g is the gravity acceleration (9.81 m/s^2). β value ranges from 0.23 to 0.7, and it is observed that it is usually decreased for a higher maximum acceleration of the ground.

$$k_h = \beta \frac{a_{max}}{g} \tag{8}$$

The average values of β for different geometry of the excavation could be presented as:

$$\beta = \begin{cases} 0.25 \text{ for H=10 m, } i\text{=60°} \\ 0.38 \text{ for H=10 m, } i\text{=75°-90°} \\ 0.43 \text{ for H=20 m, } i\text{=60°-90°} \end{cases} \tag{9}$$

Table 4. Variation of the pseudo-static coefficients in the models

Excavation height (m)	Excavation inclination (°)	PGA(g)	Min. k_h	Max k_h	Ave. k_h	β
10	60	0.2	0.06	0.08	0.07	0.35
		0.3	0.06	0.10	0.08	0.27
		0.4	0.08	0.12	0.10	0.25
		0.5	0.10	0.14	0.12	0.24
		0.6	0.12	0.16	0.14	0.23
	75	0.2	0.10	0.14	0.12	0.60
		0.3	0.10	0.16	0.13	0.43
		0.4	0.12	0.18	0.15	0.38
		0.5	0.14	0.20	0.17	0.34
		0.6	0.14	0.20	0.17	0.34
	90	0.2	0.12	0.14	0.13	0.65
		0.3	0.12	0.16	0.14	0.47
		0.4	0.14	0.16	0.15	0.38
		0.5	0.14	0.20	0.17	0.34
		0.6	0.16	0.20	0.18	0.30
20	60	0.2	0.12	0.16	0.14	0.65
		0.3	0.12	0.18	0.15	0.50
		0.4	0.14	0.20	0.17	0.43
		0.5	0.14	0.22	0.18	0.36
		0.6	0.16	0.22	0.19	0.32
	75	0.2	0.12	0.16	0.14	0.65
		0.3	0.12	0.18	0.15	0.50
		0.4	0.14	0.20	0.17	0.43
		0.5	0.16	0.22	0.19	0.38
		0.6	0.18	0.22	0.20	0.33
	90	0.2	0.12	0.16	0.14	0.70
		0.3	0.12	0.18	0.15	0.50
		0.4	0.14	0.20	0.17	0.43
		0.5	0.16	0.22	0.19	0.38
		0.6	0.18	0.22	0.20	0.33

5. Conclusion

The responses of anchored excavations under dynamic loading using harmonic time history were compared against pseudo-static analyses to examine the latter approach's ability to predict the mobilized dynamic forces in ground anchors reliably. The finite difference numerical model developed by FLAC^{2D} demonstrated good agreements with full-scale experimental results and proved to be effectively capable of simulating the stabilized excavation with pre-tensioned anchors. The applied dynamic loadings induced excess axial forces in pre-tensioned lock-off force that increased throughout the excavation depth with considerable higher magnitudes at the lower one-third of the wall height. Both dynamic and pseudo-static approaches induced axial forces in pre-tensioned lock-off load in the same manner, and the pseudo-static approach implemented in this study successfully replicated the dynamic axial forces induced in pre-tensioned anchors. Anchor spacing was found to be an important factor in mobilization of both dynamic and pseudo-static forces. Comparing the outcomes of this study with the retaining walls also revealed that higher wall flexural stiffness decreases the mobilized horizontal forces and pressure behind the retaining structure. Suggested pseudo-static coefficients effectively predict the values of the induced axial forces in anchors based on the maximum acceleration of applied dynamic load as well as the excavation geometry. An increase in the a_{max} leads to a decrease in the value of the coefficient β represented for each model. This reveals that although the pseudo-static coefficients were found to increase with the acceleration level of dynamic loads, this increase would be slighter comparing to the maximum acceleration level. Considering the severe effects of earthquakes on excavation toes, it is recommended that more reinforcement, including increasing un-bonded length of anchors or increased pre-tensioning load, should be considered for these areas.

6. Declarations

6.1. Author Contributions

Conceptualization and methodology, A.S.R.O., and M.O.; software, A.S.R.O.; validation, A.S.R.O.; formal analysis, A.S.R.O; investigation, A.S.R.O.; writing—original draft preparation, A.S.R.O.; writing—review and editing, A.S.R.O., M.O. and. H.H.; visualization, A.S.R.O. and H.H.; supervision, M.O. and H.H; All authors have read and agreed to the published version of the manuscript.

6.2. Data Availability Statement

The data presented in this study are available in article.

6.3. Funding

The author(s) received no financial support for the research, authorship, and/or publication of this article.

6.4. Conflicts of Interest

The authors declare no conflict of interest.

7. References

[1] Gazetas, G., N. Gerolymos, and I. Anastasopoulos. “Response of Three Athens Metro Underground Structures in the 1999 Parnitha Earthquake.” Soil Dynamics and Earthquake Engineering 25, no. 7–10 (August 2005): 617–633. doi:10.1016/j.soildyn.2004.11.006.

[2] Gazetas, G., E. Garini, and A. Zafeirakos. “Seismic Analysis of Tall Anchored Sheet-Pile Walls.” Soil Dynamics and Earthquake Engineering 91 (December 2016): 209–221. doi:10.1016/j.soildyn.2016.09.031.

[3] Gazetas, G, P.N Psarropoulos, I Anastasopoulos, and N Gerolymos. “Seismic Behaviour of Flexible Retaining Systems Subjected to Short-Duration Moderately Strong Excitation.” Soil Dynamics and Earthquake Engineering 24, no. 7 (September 2004): 537–550. doi:10.1016/j.soildyn.2004.02.005.

[4] Fragaszy, R. J., G. Denby, J. D. Higgins, and A. Ali. "Seismic Response of Tieback Retaining Walls (Phase I)." Final Report, No. WA-RD-138.1. (1987).

[5] Siller, Thomas J., and Dorothy D. Frawley. “Seismic Response of Multianchored Retaining Walls.” Journal of Geotechnical Engineering 118, no. 11 (November 1992): 1787–1803. doi:10.1061/(asce)0733-9410(1992)118:11(1787).

[6] Siller, Thomas J., Paul P. Christiano, and Jacobo Bielak. “Seismic Response of Tied-Back Retaining Walls.” Earthquake Engineering & Structural Dynamics 20, no. 7 (1991): 605–620. doi:10.1002/eqe.4290200702.

[7] Siller, Thomas J., and Matthew O. Dolly. “Design of Tied - Back Walls for Seismic Loading.” Journal of Geotechnical Engineering 118, no. 11 (November 1992): 1804 – 1821. doi:10.1061/(asce)0733-9410(1992)118:11(1804).

[8] Kramer, Steven Lawrence. Geotechnical earthquake engineering. Pearson Education India. (1996).

[9] Farhangi, Visar, Moses Karakouzian, and Marten Geertsema. "Effect of Micropiles on Clean Sand Liquefaction Risk Based on CPT and SPT." Applied Sciences 10, no. 9 (April 29, 2020): 3111. doi:10.3390/app10093111.

[10] Oliaei, Mohammad, and Hamid Tohidifar. "Seismic Stability of Slopes Reinforced with Sleeved and Unsleeved Piles." European Journal of Environmental and Civil Engineering 24, no. 8 (March 12, 2018): 1091–1119. doi:10.1080/19648189.2018.1447515.

[11] Peng, Ningbo, Yun Dong, Ye Zhu, and Jie Hong. "Influence of Ground Motion Parameters on the Seismic Response of an Anchored Rock Slope." Edited by Castorina S. Vieira. Advances in Civil Engineering 2020 (December 23, 2020): 1–10. doi:10.1155/2020/8825697.

[12] Dram, Abdelkader, Sadok Benmebarek, and Umashankar Balunaini. "Performance of Retaining Walls with Compressible Inclusions Under Seismic Loading." Civil Engineering Journal 6, no. 12 (December 1, 2020): 2474–2488. doi:10.28991/cej-2020-03091631.

[13] Farrokhzad, Farzad, SeyedArmin MotahariTabari, Hamid Abdolghafoorkashani, and Hamidreza Tavakoli. "Seismic Behaviour of Excavations Reinforced with Soil–Nailing Method." Geotechnical and Geological Engineering (April 7, 2021). doi:10.1007/s10706-020-01625-7.

[14] Tiwari, R. C., N. P. Bhandary, and R. Yatabe. "3-D Elasto-Plastic SEM Approach for Pseudo-Static Seismic Slope Stability Charts for Natural Slopes." Indian Geotechnical Journal 44, no. 3 (November 16, 2013): 305–321. doi:10.1007/s40098-013-0086-y.

[15] Panah, Ali Komak, and Sina Majidian. "2D Numerical Modelling of Soil-Nailed Structures for Seismic Improvement." Geomechanics and Engineering 5, no. 1 (February 25, 2013): 37–55. doi:10.12989/gae.2013.5.1.037.

[16] Sabatini, P. J., D. G. Pass, and Robert C. Bachus. Ground anchors and anchored systems. No. FHWA-IF-99-015. United States. Federal Highway Administration. Office of Bridge Technology. (1999)

[17] Donovan, K., W. G. Pariseau, and M. Cepak. "Finite element approach to cable bolting in steeply dipping VCR stopes." Geomechanics application in underground hardrock mining (1984): 65-90.

[18] Kuhlemeyer, Roger L., and John Lysmer. "Finite element method accuracy for wave propagation problems." Journal of the Soil Mechanics and Foundations Division 99, no. 5 (1973): 421-427.

[19] Duncan, James M., and Chin-Yung Chang. "Nonlinear analysis of stress and strain in soils." Journal of Soil Mechanics & Foundations Div 96(5), (1970):1629-1653.

[20] Seed R. B. Duncan J.M. A. "finite element analysis program for evaluation of soil-structure interaction and compaction effects", Department of Civil Engineering, University of California (1984).

[21] Namjoo, Amir Mostafa, Mohammad Mohsen Toufigh, and Vahid Toufigh. "Experimental Investigation of Interface Behaviour Between Different Types of Sand and Carbon Fibre Polymer." European Journal of Environmental and Civil Engineering (June 12, 2019): 1–20. doi:10.1080/19648189.2019.1626290.

[22] Namjoo, Amir Mostafa, Khashayar Jafari, and Vahid Toufigh. "Effect of Particle Size of Sand and Surface Properties of Reinforcement on Sand-Geosynthetics and Sand–carbon Fiber Polymer Interface Shear Behavior." Transportation Geotechnics 24 (September 2020): 100403. doi:10.1016/j.trgeo.2020.100403.

[23] Farhangi, Visar, and Moses Karakouzian. "Effect of Fiber Reinforced Polymer Tubes Filled with Recycled Materials and Concrete on Structural Capacity of Pile Foundations." Applied Sciences 10, no. 5 (February 25, 2020): 1554. doi:10.3390/app10051554.

[24] Cundall, P. A. "FLAC manual: A computer program for Fast Lagrangian Analysis of Continua." First Revision August (2001).

[25] Briaud, Jean-Louis, and Yujin Lim. "Tieback Walls in Sand: Numerical Simulation and Design Implications." Journal of Geotechnical and Geoenvironmental Engineering 125, no. 2 (February 1999): 101–110. doi:10.1061/(asce)1090-0241(1999)125:2(101).

[26] Briaud, J. L. "National geotechnical experimentation sites at Texas A&M University: Clay and sand data collected until 1992." Department of Civil Engineering, Texas A&M University, College Station, TX, USA. Report No. NGES-TAMU-001, (1993).